Screening in a two-band model for superconducting infinite-layer nickelate

Tharathep Plienbumrung [1,2] Maria Daghofer [1,2] Michael Schmid [3] and Andrzej M. Oleś [4,5,*]

[1] *Institute for Functional Matter and Quantum Technologies, University of Stuttgart, Pfaffenwaldring 57, D-70550 Stuttgart, Germany*
[2] *Center for Integrated Quantum Science and Technology, University of Stuttgart, Pfaffenwaldring 57, D-70550 Stuttgart, Germany*
[3] *Waseda Research Institute for Science and Engineering, Waseda University, Okubo, Shinjuku, Tokyo 169-8555, Japan*
[4] *Max Planck Institute for Solid State Research, Heisenbergstrasse 1, D-70569 Stuttgart, Germany*
[5] *Institute of Theoretical Physics, Jagiellonian University, Profesora Stanisława Łojasiewicza 11, PL-30348 Kraków, Poland*

(Received 19 October 2021; revised 26 September 2022; accepted 27 September 2022; published 10 October 2022)

Starting from an effective two-dimensional two-band model for infinite-layered nickelates, consisting of bands obtained from d- and s-like orbitals, we investigate to which extent it can be mapped onto a single-band Hubbard model. We identify screening of the more itinerant s-like band as an important driver. In the absence of screening one strongly correlated band gives an antiferromagnetic ground state. For weak screening, the strong correlations push electrons out of the s band so that the undoped nickelate remains a Mott insulator with half-filled d orbitals. This regime markedly differs from the observations in high-T_c cuprates and pairing with s-wave symmetry would rather be expected in the superconducting state. In contrast, for strong screening, the s and $d_{x^2-y^2}$ bands are both partly filled and couple only weakly, so that one approximately finds a self-doped d band as well as tendencies toward d-wave pairing. Particularly in the regime of strong screening mapping to a one-band model gives interesting spectral weight transfers when a second s band is also partly filled. We thus find that both one-band physics and a Kondo-lattice-like regime emerge from the same two-orbital model, depending on the strength of electronic correlations and the size of the s-band pocket.

DOI: 10.1103/PhysRevB.106.134504

I. INTRODUCTION

The recent discovery of superconductivity in infinite-layer $NdNiO_2$ thin films with Sr doping [1] has rekindled interest in Ni-based superconductivity. The interest arises mostly because they can be assumed to be strongly correlated and thus in some respect similar to cuprate superconductors. The two families of compounds also have similar lattices, with either CuO_2 or NiO_2 planes that give them a predominantly two-dimensional (2D) character. Analyzing the NiO_2 layer in analogy to a CuO_2 layer, one expects Ni^{1+} with a d^9 electronic configuration, and in both cases expects antiferromagnetic (AFM) superexchange interactions [2–4]. Indeed, magnetic excitations in undoped nickelates reveal such AFM correlations [5,6].

However, the parent compound $RNiO_2$ (R = La, Nd) does not show any signs of magnetic ordering [7,8] at low temperatures down to 1.5 K. Moreover, both the insulating NiO_2 layer [2,3,9,10] and band-structure calculations [11–18] suggest that other orbitals or bands might be relevant.

Several approaches suggest that a two-band model should be a realistic starting model for doped infinite-layer nickelates [19–24]. It faithfully represents the strongly correlated $x^2 - y^2$ orbital at Ni ions and the s orbital which collects all remaining contributions from other orbitals. Indeed, two bands cross the Fermi energy as shown in Fig. 1. Accordingly, a large variety of potential pairing symmetries have been presented [9], among them s- and d-wave states [10,13] as well as even more exotic $s + id$ pairing [25]. However, alternatively, single-band [26] and three-band [13,24] models have been proposed. Experimentally, d-wave symmetry was reported, as was s-wave [27,28].

Microscopically, two main differences between Cu- and Ni-based superconductors are (i) larger Ni-O charge-transfer energy compared to Cu-O, and (ii) the presence of highly dispersive rare-earth bands in the layered nickelates [4,29]. In cuprates, doped holes go mostly into oxygen sites, where they form Zhang-Rice singlets with the half-filled $Cu(d_{x^2-y^2})$ states [30]. Due to the larger charge-transfer energy raising the energy of the oxygen orbitals, Ni-O hybridization is less important and doped holes likely reside on Ni sites in doped $Nd_{1-x}Sr_xNiO_2$ [2,3,31–33]. While oxygen states can thus be assumed to play less of a role [26], the question of the orbital character of doped holes remains and is affected by the rare-earth band. This band hybridizes with Ni apical states, thus obtaining some $Ni(d_{3z^2-r^2})$ and $Ni(d_{xy})$ character, and forms a hybrid "axial" s orbital [19]; see Fig. 1. Depending on where doped holes go, one can expect either that almost only the $d_{x^2-y^2}$ states are relevant [26], or that half-filled more localized $d_{x^2-y^2}$ states together with itinerant s-like carriers

*Corresponding author: a.m.oles@fkf.mpi.de

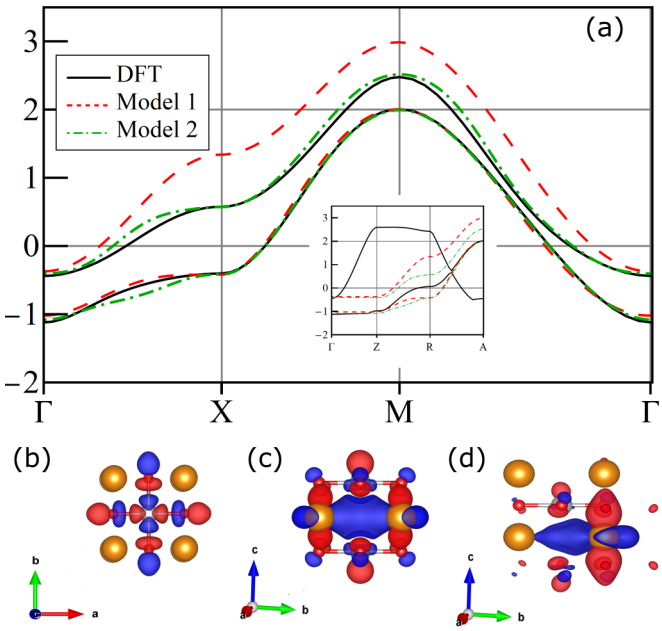

FIG. 1. Noninteracting band structure of $NdNiO_2$: (a) Density-functional theory (DFT) bands crossing the Fermi surface (black) and two 2D tight-binding models obtained by projecting a Wannier fit onto the plane along 2D path (red dashed and green dotted). The Fermi energy $E = \mu$ corresponds to the DFT electronic structure. Inset shows the DFT band structure along three-dimensional path Γ-Z-R-A. Wannier orbitals are also shown: (b) The "$d_{x^2-y^2}$-like" orbital making up the lower band of model 1; the corresponding orbital of model 2 looks the same. The "s-like" orbitals of models 1 and 2 are given in (c) and (d).

form a Kondo-lattice-like two-band system [4,16,25,32], or that both scenarios have their point [34].

The purpose of this paper is to investigate how similar cuprate and nickelate superconductivities are, i.e., whether and where multiband effects come into play. We find that screening is a crucial variable and that the two bands (Fig. 1) can mix considerably at intermediate screening, where pairing with s-wave symmetry would be expected. Both for very weak and for strong screening, however, the bands mostly decouple and the effective physics becomes similar to a single Hubbard band [26]. We then find a Mott insulator (doped band with potential d-wave pairing) for strong (weak) correlations. Correlation strength thus emerges as an important factor in the description of nickelate superconductors.

The remaining of this paper is organized as follows. The two-band model arises from the electronic structure calculations as described in Sec. II A, where Fig. 1 also shows that the dispersion close to the Fermi level can be described similarly well with quite different Wannier functions [35,36]. Hoppings in the corresponding parametrizations of the kinetic energy are, however, rather similar so that consistent results can be obtained that are independent of the choice of the fit. Electronic interactions are given by two Kanamori parameters $\{U_\alpha, J_H\}$ and we discuss their screening in Sec. II B. Here, the fact that kinetic energy of the rare-earth-dominated band can be described similarly well with rather different Wannier functions presents more of a challenge. The different shape of the orbitals suggests that overlap integrals determining electronic correlations might also differ substantially. We thus opt to investigate a very wide range of potential regimes going from weak to very strong correlations in Sec. III. Results from exact diagonalization are presented for the density distribution and spin correlations (Sec. III A) and for the spectral density (Sec. III B). We search for superconducting (SC) phases both in hole-doped and electron-doped systems in Sec. IV A. Next we present phase diagrams of infinite-layer nickelates in (U_d, α) planes in Sec. IV B. Two SC compounds, $NdNiO_2$ and $LaNiO_2$, are compared in Sec. IV C. The paper is concluded in Sec. V.

II. TWO-BAND MODEL AND METHODS

A. Kinetic energy

We start from the kinetic energy in the electronic structure. The DFT band structure, see Fig. 1, is calculated with the QUANTUM ESPRESSO code [37–39] using a plane-wave pseudopotential method [40]; similar calculations were performed previously [19,29,31]. In Fig. 1(a), one finds that two bands cross the Fermi level. Wannier-orbital models were obtained to reproduce the two bands crossing the Fermi level. In both cases, the Wannier orbital corresponding to the lower band contains substantial Ni($d_{x^2-y^2}$) contributions, with some weight on the surrounding O atoms; see Fig. 1(b). The upper band is formed by a rather extended s-like state as illustrated, where Nd($5d$) orbitals hybridize with Ni(s) as well as Ni(d_{xy}) and Ni($d_{3z^2-r^2}$) states. Both are compromises to some extent: one of the fits (model 2) has a smaller imaginary part, but the orbitals of the other (model 1) more closely respect the expected symmetries; see Figs. 1(c) and 1(d). Hoppings are, however, very similar.

The feature of the band structure that most distinguishes nickelates from cuprates is the electron pockets formed by the upper s-like band around the Γ and A points in the Brillouin zone. In the DFT band structure, they contain $\approx 7\%$ of the occupied states [29], which in turn implies that there are hole carriers [32] in the $x^2 - y^2$ band even without Sr doping. While 7% self-doping may not seem much, it is in line with the 5% of Sr doping needed to destroy antiferromagnetism in a cuprate superconductor La_2CuO_{4-y} [41]. The Γ pocket lying about -0.4 eV below the Fermi level appears thus to be an important feature when constructing an effective model.

The Wannier90 interface [42] gives the parametrization

$$H_{\rm kin} = \sum_{i\alpha\sigma} \epsilon_\alpha d^\dagger_{i\alpha\sigma} d_{i\alpha\sigma} + \sum_{ij\alpha\beta\sigma} t^{\alpha\beta}_{ij} d^\dagger_{i\alpha\sigma} d_{j\beta\sigma} \qquad (1)$$

of these two bands, where $d_{i\alpha\sigma}$ ($d^\dagger_{i\alpha\sigma}$) is an electron annihilation (creation) operator at site i for orbital α and spin σ. $\alpha = d$ denotes the Ni(x^2-y^2)-dominated state of Fig. 1(b), and $\alpha = s$ stands for the extended s-like state of Fig. 1(c). Hopping parameters $t^{\alpha\beta}_{ij}$ and on-site energies ϵ_α are given in the Supplemental Material (SM) [43] for two slightly different Wannier projections.

With exact diagonalization and the Lanczos algorithm [44], we can address an eight-site cluster, e.g., the $2 \times 2 \times 2$ cluster that was used to investigate magnetic order [45]. We are here mostly interested in electronic correlations, which

predominantly affect the d band (see discussion below). As this band has nearly no dispersion along the z direction, see inset of Fig. 1(a), we use instead a $\sqrt{8} \times \sqrt{8}$ cluster in the (x, y) plane. We thus need a 2D projection of the band structure, which we obtained by a fit that can in turn be motivated by twisted boundary conditions (TBCs) [46–48]. The resulting 2D bands are shown in Fig. 1(a); hopping parameters and details of the procedure are given in the SM [43]. This was done for both Wannier projections, leading to two similar effective two-dimensional two-band models, whose main differences concern the upper band. As can be seen in the SM [43], results of both models are very similar, so that we focus the main part of the paper on the model 1.

B. Interactions and screening effect

Electronic interactions are taken to be on-site, i.e.,

$$H_{\rm int} = \sum_{i\alpha} U_\alpha n_{i\alpha\uparrow} n_{i\alpha\downarrow} + \left(U' - \frac{J_H}{2}\right) \sum_i n_{id} n_{is} - 2J_H \sum_i \vec{S}_{id} \cdot \vec{S}_{is} + J_H \sum_i (d^\dagger_{id\uparrow} d^\dagger_{id\downarrow} d_{is\downarrow} d_{is\uparrow} + \text{H.c.}). \quad (2)$$

$n_{i\alpha\sigma}$ is the electron number operator at site i, orbital α, and spin σ, and $\{\vec{S}_{i\alpha}\}$ is the corresponding spin operator. Intraorbital Coulomb repulsion $U_{\alpha=s/d}$ depends on the band α; Hund's exchange J_H and interorbital repulsion U' couple the bands.

Upper limits for the "bare" U_d and J_0 are given by their atomic values $U_d \approx 8$ eV and $J_0 \approx 1.2$ eV, which would be applicable to a NiO_2 model for an insulating layer [2,3]. However, even though Ni-O hybridization is expected to be weaker than in cuprates (due to larger Ni-O crystal-field splitting), it is still present, see the orbital wave function in Fig. 1(b), and expected to substantially reduce effective values [3,30]. Note that U_s cannot be related to atomic values for Ni, as the s-orbital is not even centered on a Ni site [19]. Coulomb interactions are thus expected to be weaker in the s-like band because the wave function is far more extended and largely of Nd $5d$ character; see Fig. 1(c). While the Coulomb repulsion U_d is almost unscreened in the correlated $x^2 - y^2$ orbitals, considerable screening occurs for s orbitals. One thus expects $U_d > U_s$ and we introduce here parameter $\alpha \in [0, 1]$ so that

$$U_s = \alpha U_d, \quad J_H = \alpha J_0, \quad U' = U_s - 2J_H. \quad (3)$$

Approaches like the constrained random-phase approximation might provide estimates for the screened interaction parameters; however, this is not straightforward. Even though, as shown above, the two Wannier-projection schemes used lead to very similar band structures, and thus hopping integrals, the orbital wave function of the upper band differs substantially. This would in turn affect effective interactions, so that we opt here for a model approach, where we investigate which physics can be expected for various screening scenarios. The parametrization of Eq. (3) is used here as the simplest approach capturing the essential features of the electronic structure, i.e., the interplay of a more and a less correlated band.

The full Hamiltonian $H = H_{\rm kin} + H_{\rm int}$ thus describes a correlated 2D band, which is strongly reminiscent of cuprates, but that moreover interacts with a more itinerant rare-earth band. By accepting some electrons, the itinerant s band not only dopes the correlated d band, but also contains itinerant carriers [19,31,32]. We are next going to investigate the impact of these carriers and their remaining correlations.

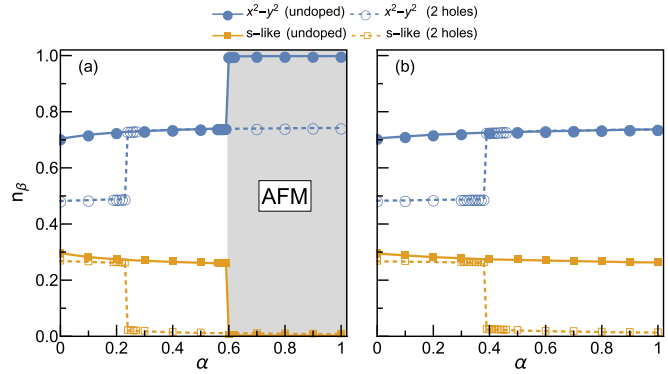

FIG. 2. Orbital electron density (4) as a function of screening parameter α with $J_0/U_d = 0.15$ for (a) $U_d = 8.0$ and $J_0 = 1.2$; (b) $U_d = 4.0$ and $J_0 = 0.6$. Solid (dashed) line for eight (six) electrons, i.e., undoped and doped with two holes in Ni_8O_{16} units.

III. NUMERICAL RESULTS

A. Density of states and spin correlations

First we look at orbital densities,

$$n_\alpha = \frac{1}{N_s} \sum_{i\sigma} \langle d^\dagger_{i\alpha\sigma} d_{i\alpha\sigma} \rangle, \quad (4)$$

where $N_s = 8$ is the number of lattice sites, $\alpha = s, d$, and the average is obtained for the ground state with 8 (6) electrons. In the two-band model the undoped compound corresponds to quarter filling, i.e., eight electrons. For very strong interactions, band dispersion is suppressed and on-site energies dominate, so that the $x^2 - y^2$ orbital becomes half filled. This is indeed observed for strong $U_d = 8$ eV and $J_0 = 1.2$ eV; see Fig. 2(a). The spin-structure factor is here strongly peaked at (π, π), see Fig. 3(a), so that we recover the familiar picture of a half-filled AFM Mott insulator [49]. However, we are in the metallic regime and finite electron density is found in the s orbital for the uncorrelated band structure of Fig. 1(a).

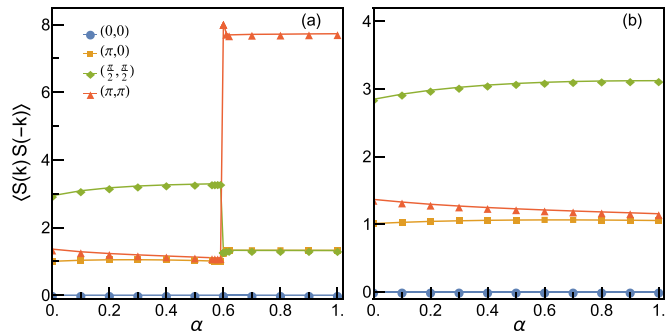

FIG. 3. Spin structure factor of undoped system as a function of screening parameter α with $J_0/U_d = 0.15$ for (a) $U_d = 8.0$ and $J_0 = 1.2$; (b) $U_d = 4.0$ and $J_0 = 0.6$.

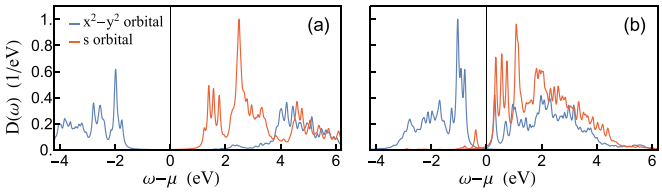

FIG. 4. Density of states $D(\omega)$ of undoped nickelate with unscreened interactions ($\alpha = 1$). Fermi energy is set to zero; the densities are normalized to one (per spin). Intraorbital Coulomb interaction in Eq. (2) is selected at (a) $U_d = 8$ eV and (b) $U_d = 4$ eV.

Figure 2 shows the orbital-resolved density versus screening parameter α. Here we interpolate between the strongly correlated and uncorrelated regimes, while keeping a physically plausible hierarchy of interactions: $U_s = \alpha U_d < U_d \leqslant 8$ eV. (For the moment, we keep the ratio $J_0/U_d = 0.15$ constant.) In Fig. 2(a), U_d is at its upper limit 8 eV, and for weak to moderate screening, we find a half-filled $x^2 - y^2$ orbital with AFM order. However, as soon as U_s is screened by about 40%, self-doping occurs and some electrons enter the s band. The same happens for—presumably more realistic—$U_d = 4$ eV, even without additional screening. The presence of the second band thus causes the loss of long-range magnetic order even for parameter regimes where the $x^2 - y^2$ orbital by itself would lead to an insulator.

The next question to ask is where holes doped into the quarter-filled system go. Three regimes emerge; see Fig. 2. First, in the weakly screened Mott insulator and for large U_d, the state is AFM and holes naturally enter only the $x^2 - y^2$ orbital. In contrast, the second regime is found at intermediate screening [$\alpha \simeq 0.5$; see Fig. 2(a)], or for interactions that are reduced from the outset; see Fig. 2(b). Finally, in the third regime of strong screening ($\alpha < 0.5$), hole doping happens again into the $x^2 - y^2$ orbital, with the s electrons remaining unaffected.

Figure 3 shows the spin-structure factor of undoped nickelate at four momenta k accessible to the $\sqrt{8} \times \sqrt{8}$-site cluster. In the unscreened limit, see Fig. 3(a), the AFM wave vector (π, π) dominates for $\alpha > 0.6$, highlighting the AFM Mott insulator in the strongly interacting limit. Upon decreasing $\alpha < 0.6$, the strongest signal is found at $(\frac{\pi}{2}, \frac{\pi}{2})$, but its dominance is far less pronounced. Similarly, in Fig. 3(b), the strongest signal at (π, π) is suppressed once interactions in the $x^2 - y^2$ orbital are weaker.

B. One-particle spectral density

To understand the occurrence of a possible SC phase in infinite-layer nickelates we consider first the one-particle spectra in the normal phase. When interactions are unscreened ($\alpha = 1$), the undoped system is a Mott insulator for $U_d \geqslant 4$ eV; see Fig. 4. For $U_d = 8$ eV one finds that the correlated d band is half filled and a broad gap $\sim$3.5 eV separates occupied from empty states, with the Fermi energy within the gap; see Fig. 4(a). The gap in the correlated band consisting of $x^2 - y^2$ orbitals is close to 6 eV and unoccupied states above the Fermi level are the s-band states. This electronic structure corresponds to an AFM Mott insulator.

When $U_d = 4$ eV, the gap in the correlated band decreases to $\sim$1.0 eV but the tail of the s band falls below the Fermi energy which still separates the occupied and unoccupied states; see Fig. 4(b). However, for this value of U_d, we cannot exclude a metallic phase, with a small fraction of electrons occupying the s states in the thermodynamic limit.

The different behavior in the three regimes mentioned in Sec. III A is also reflected in the single-particle spectra shown in Fig. 5. Filling corresponds to doping with two holes and the TBC is used to resolve more momenta [46–48]. Both for very strong $U_d = 8$ eV [panels (a) and (b)] and for moderate interactions $U_d = 4$ eV [panels (c) and (d)] (including also weaker screening with $\alpha = 0.5$) the correlations induce a gap in the $x^2 - y^2$ band [50]. The lowest states for electrons are then in the s band, so that going toward the undoped regime involves doping the s band. Spectra taken at quarter filling lead to analogous interpretations. This can be seen in Fig. 4, where we show the density of states for eight electrons (i.e., quarter filling). Data were obtained by means of TBCs, integrating over five sets of boundary conditions.

At strong screening (i.e., for weak s-orbital interactions), both $x^2 - y^2$ and s states are occupied and can appear quite close to the Fermi energy regardless of the value of U_d; see Figs. 5(a) and 5(c). Surprisingly, the spectra shown in Figs. 5 depend little on U_d and stronger on the screening. At strong screening when $\alpha = 0.2$, the occupied states in the $x^2 - y^2$ band are rather similar for $U_d = 8$ eV and $U_d = 4$ eV, except that the curvature of the occupied states changes along the $(\pi, 0)$-$(0, \pi)$ line. Since this implies that interactions U' and J_H between the d and s states here do not play a significant role, it supports the notion of a correlated (and doped) d band that is only affected by a metallic s band via self-doping.

In contrast, for stronger correlations, i.e., weaker screening $\alpha = 0.5$, spectra shown in Figs. 5(b) and 5(d) are affected by U_d. All electrons are here in the correlated $x^2 - y^2$ states. It is remarkable that the occupied states fall almost at the same energies, independently of whether $U_d = 8$ eV or $U_d = 4$ eV [cf. Figs. 6(a) and 6(b) and Figs. 6(c) and 6(d)]. However, splitting between the d and s states is clearly affected by U_d (via U' and J_H), which indicates that the s and d bands are in this regime directly coupled, not only via self-doping.

Analogous conclusions can be drawn from the undoped density of states shown in Fig. 6, where Figs. 6(a) and 6(c) are extremely similar: In the regime of strong screening, both bands are partially filled and results hardly depend on U_d at all. As already discussed for Figs. 5(a) and 5(c), this suggests that correlations between the two bands do here not play a significant role. In the intermediate regime on the other hand, both bands are likewise partially filled. The comparison with Figs. 5(b) and 5(d) indicates that the s states being close to the Fermi level could be doped away. In this regime, results depend on U_d, indicating that correlations are here more important to describe low-energy features close to the Fermi level.

Interestingly, the screening increases the density of s electrons and simultaneously n_d decreases as in the undoped case $n_d + n_s = 1$. This makes the lower Hubbard band (LHB) less than half filled and considerable spectral weight is transferred from the upper Hubbard band (UHB) to the unoccupied part of the LHB (i.e., above the Fermi level μ and below the gap). The

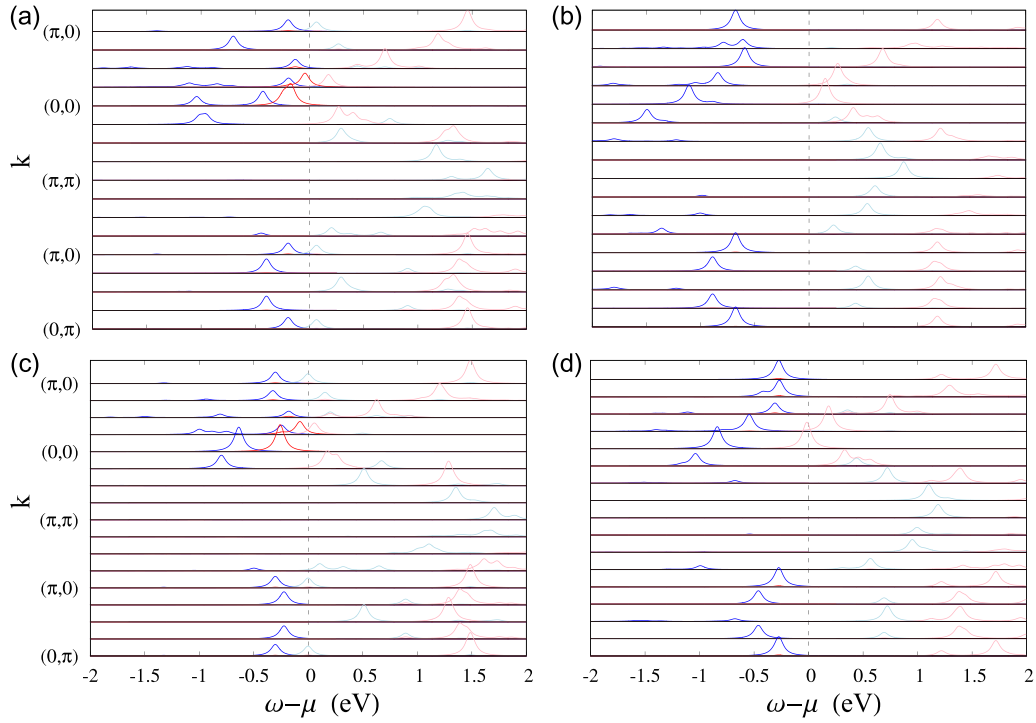

FIG. 5. Single-particle spectra for six-electron system obtained with TBCs and $J_0/U_d = 0.15$. Top: $U_d = 8$ eV and (a) $\alpha = 0.2$, (b) $\alpha = 0.5$; bottom: $U_d = 4$ eV and (c) $\alpha = 0.2$, (d) $\alpha = 0.5$. Blue (red) spectra below μ correspond to occupied $x^2 - y^2$ and s states, respectively. Light spectra above μ are for empty states in both bands.

mechanism of such a spectral weight transfer is well known in the partly filled Hubbard model [51,52] and it explains why the weight of the LHB exceeds 0.500 per spin. Here doping in the Mott insulator is mimicked by the partial filling of the s band. The largest transfer of spectral weight is found at $U_d = 4$ eV and $\alpha = 0.5$; see Table I. The UHB forms only in the correlated $x^2 - y^2$ band and no Hubbard subbands form within the s band even at $U_d = 8$ eV.

Altogether, the densities of states $D(\omega)$ give a metallic regime for intermediate ($\alpha = 0.5$) and strong ($\alpha = 0.2$) screening of strongly correlated $x^2 - y^2$ states; see Fig. 6. A large gap between the Hubbard subbands opens when $U_d = 8$ eV; this gap is reduced to ∼0.5 eV when $U_d = 4$ eV. Nevertheless the system has still a gap which separates the Hubbard subbands. The electronic structure for the $x^2 - y^2$ band is typical for a doped Mott insulator, with the weight of the UHB reduced by the kinetic processes in a doped system [51,52]. Indeed, the weight in the LHB above the Fermi energy increases by $\sim 2\delta$ where δ stands for the doping in the LHB, which would also be the weight transferred from the UHB to the LHB by finite doping. In this regime the s band is only weakly correlated and Hubbard subbands are not visible.

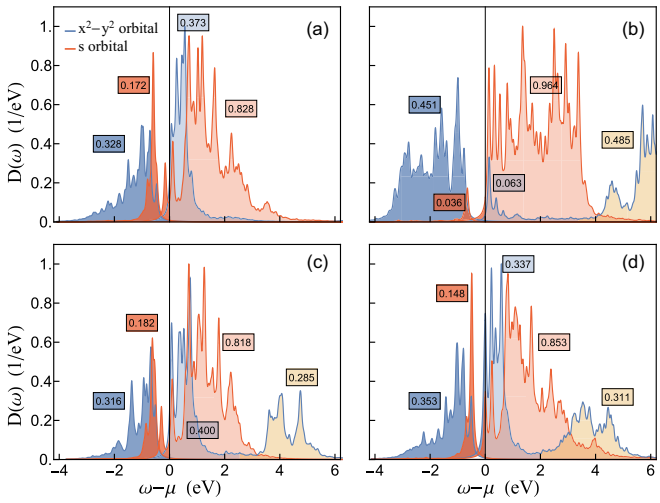

FIG. 6. Density of states $D(\omega)$ of undoped nickelate for weak and moderate screening with $\alpha = 0.2$ and $\alpha = 0.5$: (a), (b) $U_d = 8$ eV; (c), (d) $U_d = 4$ eV. The conventions are the same as in Fig. 4.

IV. PAIRING SYMMETRY

A. Search for superconducting correlations

To investigate pairing symmetries we calculate ground state overlaps [53,54] between the undoped ground state ($N = 8$) and the one with two holes ($N = 6$), i.e., $\langle \Phi(N=8)|\Delta_n|\Phi(N=6)\rangle$, where $|\Phi(N)\rangle$ is the ground state for N electrons. Pairing operator $\Delta_{s/d}$ corresponds to s- and d-wave symmetry,

$$\Delta_{s/d} = \sum_{\substack{i,\mu,\sigma\neq\sigma' \\ \lambda=-1,1}} d^\dagger_{i\mu,\sigma}\left(d^\dagger_{i+\lambda\hat{x},\mu,\sigma'} \pm d^\dagger_{i+\lambda\hat{y},\mu,\sigma'}\right), \qquad (5)$$

where μ labels $x^2 - y^2$ and s orbitals and the $+$ ($-$) sign refers to s-wave (d-wave) pairing. $\hat{x}$ ($\hat{y}$) point to nearest neighbors in the x (y) direction. We consider here only intraorbital pairs, as we found interorbital weight to be negligible.

For strong interactions $U_d = 8$ eV and $\alpha > 0.6$, where the undoped ground state is an AFM insulator, neither pairing can

TABLE I. Electron densities n_d and n_s per spin obtained in the undoped nickelate for screened interactions ($\alpha < 1$). The weight of the LHB $w_{\rm LHB}$ is increased by the kinetic weight transfer from the UHB [51,52].

U_d (eV)	α	n_d	n_s	$w^{>}_{\rm LHB}$	$w_{\rm LHB}$
8.0	0.20	0.328	0.172	0.373	0.701
	0.50	0.451	0.036	0.063	0.514
4.0	0.20	0.316	0.182	0.400	0.716
	0.50	0.353	0.148	0.337	0.690

be found; the doped holes here prefer to be further apart. In the intermediate regime, where doped holes were found to prefer the s-like orbital, s-wave pairing is found; see Fig. 7. The $x^2 - y^2$ orbital does here not participate in the pairing. The regime would thus be best described with a Kondo-lattice-like model, where the $x^2 - y^2$ orbital provides spins and the s-like band itinerant carriers [4,16,25,32].

On the other hand, for strong screening, the pairing is of d-wave symmetry and the involved holes are in the $x^2 - y^2$ states. Both the doped and undoped ground states contain here finite electron density in the s-like band, but their contribution to the pairing is small; see the open squares in Fig. 7. Most of the weight is found in pairs made up of $d_{x^2-y^2}$ holes. In this regime, the s-like band does not play an important role [26]; its main effect is to increase hole concentration in the $x^2 - y^2$ states via self-doping.

In addition to hole-doped $NdNiO_2$, electron-doped $NdNiO_2$ is discussed in Fig. 8, which shows the overlaps involving the states with 10 and 8 electrons. In the strongly correlated regime $\alpha > 0.5$, where the undoped system is an AFM with half-filled $x^2 - y^2$ orbital, we find a tendency toward s-wave pairs formed by s-band electrons. We find no pairing for stronger screening $\alpha < 0.5$ or for $U_d = 4$ eV, in stark contrast to hole doping. The reason is that the $x^2 - y^2$ orbital of the undoped system is here only partially filled: extra electrons then enter the $x^2 - y^2$ band; see also the unoccupied states in Figs. 6(a) and 6(b) and Figs. 6(c) and 6(d). This moves the $x^2 - y^2$ orbital toward half filling and favors AFM order [55–58] rather than superconductivity.

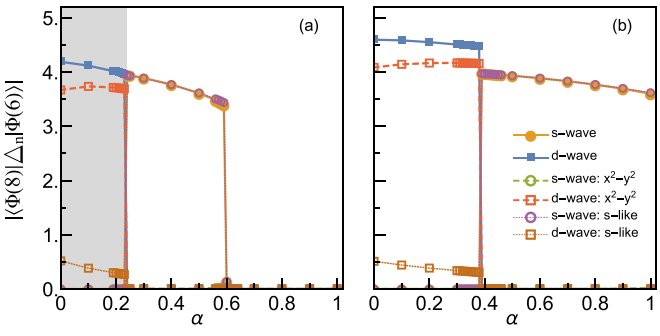

FIG. 7. Ground state overlap $\langle\Phi(8)|\Delta_n|\Phi(6)\rangle$ as a function of screening parameter α for (a) $U_d = 8$ eV, $J_0 = 1.2$ eV; (b) $U_d = 4$ eV, $J_0 = 0.6$ eV. Solid lines indicate s- and d-wave symmetries; dashed (dotted) line for $x^2 - y^2$ (s) orbital. The shaded region indicates the region with some triplet tendencies (see text).

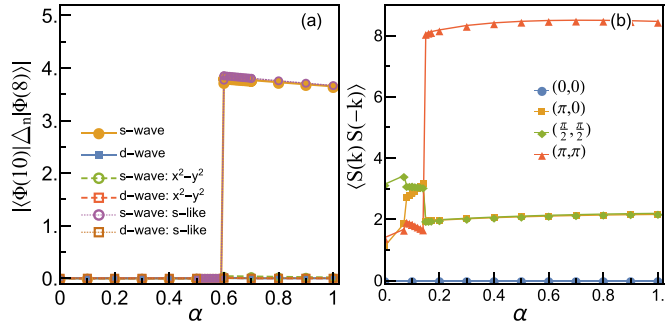

FIG. 8. Ground state of electron-doped superconductors for $U_d = 8$ eV, $J_0 = 1.2$ eV: (a) Ground state overlap $|\langle\Phi(8)|\Delta_n|\Phi(10)\rangle|$ as a function of screening parameter α for s-wave and d-wave symmetry, see legend, and (b) spin structure factor $\langle S(k)S(-k)\rangle$ at selected special points of high symmetry, see legend, and for a filling of 10 electrons.

B. Phase diagram

We now turn to the influence of Hund's exchange coupling and collect information on pairing symmetries, displayed in the phase diagrams presented in Fig. 9. For strong and unscreened Coulomb repulsion and not too strong Hund's exchange coupling, the undoped system shows AFM order and no sign of pairing. In this regime, the s-like band is empty and the $x^2 - y^2$ band is half filled and Mott insulating; see Figs. 2(a) and 4. For weaker correlations (intermediate screening), AFM order is replaced by s-wave pairing (practically

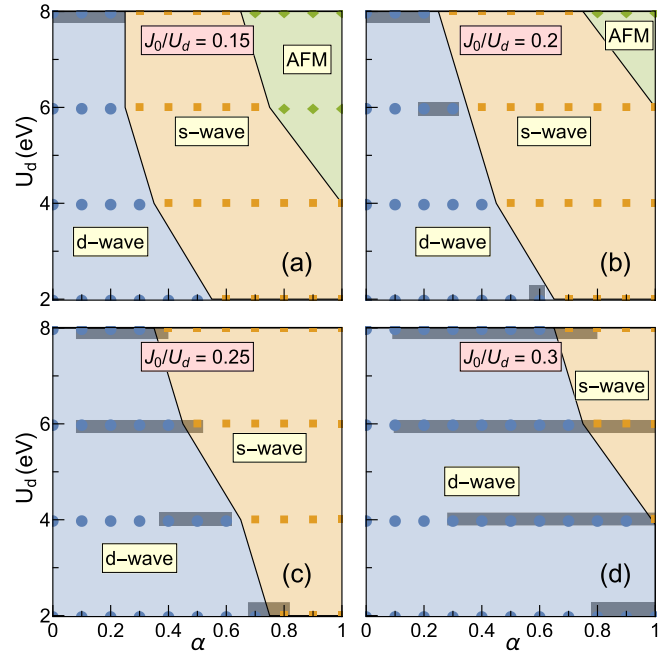

FIG. 9. $NdNiO_2$ phase diagram in (U_d, α) plane for increasing Hund's exchange, i.e., increasing ratio J_0/U_d: (a) $J_0/U_d = 0.15$ (as used above); (b) $J_0/U_d = 0.2$; (c) $J_0/U_d = 0.25$; (d) $J_0/U_d = 0.3$. Triplet tendencies are indicated by gray shading. For $J_0/U_d \geqslant 0.25$ in (c) and (d) AFM order vanishes and the phase diagram contains only SC phases. Note that the lowest value of U_d used (i.e., y-axis offset) is 2 eV.

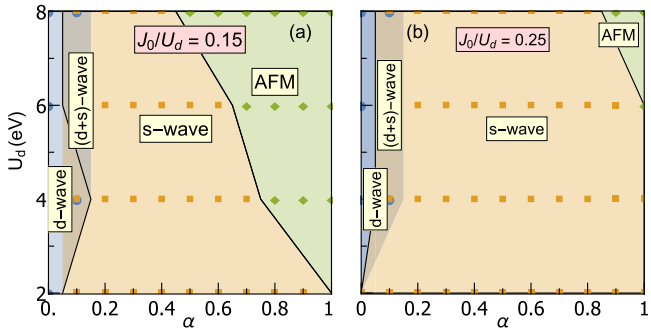

FIG. 10. Phase diagram for $LaNiO_2$ under hole doping in the (U_d, α) plane obtained for (a) $J_0/U_d = 0.15$ and (b) $J_0/U_d = 0.25$.

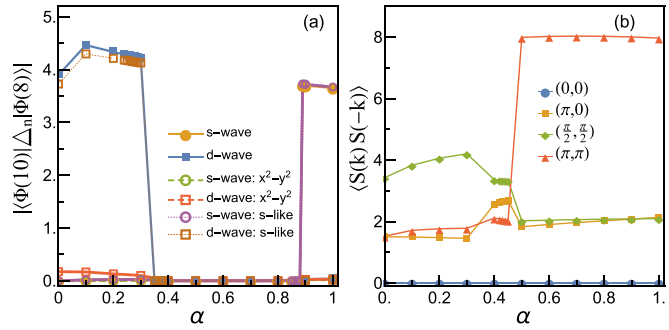

FIG. 11. Electron doping for $LaNiO_2$ depending on screening α and for $J_0/U_d = 0.15$, $U_d = 4$ eV. The panels show (a) ground state overlap with two electrons added to quarter filling and (b) spin structure factor for 10 electrons.

only involving s-band holes), while d-wave pairing arises at strong screening. In this last regime, some electrons are found in the s-like band, but the doped holes enter the $x^2 - y^2$ band, see Fig. 2, and pairing involves mostly the $x^2 - y^2$ orbital. Figure 9 illustrates that stronger Hund's-exchange pairing reduces effective correlations, suppresses AFM order, and promotes d-wave pairing.

In addition to the AFM phase and s-wave or d-wave pairings, we find some indications of triplet pairing, especially at stronger Hund's exchange coupling, see Figs. 9(c) and 9(d), but also for very strong bare on-site interaction $U_d = 8$ eV, see Fig. 9(a). Energies obtained for doping with one $\uparrow$ and one $\downarrow$ hole are here degenerate with the energies obtained with two $\uparrow$ holes, indicating that the doped pair is a triplet. In order to check the stability of this result, we also used TBCs. The degeneracy is then lifted and the $S^z = 0$ state has lower energy, suggesting that triplet pairing might be a finite-size effect. Moreover, the needed Hund's exchange would be rather large ($J_0/U_1 \gtrsim 0.25$).

C. $LaNiO_2$ versus $NdNiO_2$

Furthermore, the electronic properties of the $LaNiO_2$ compound are obtained starting from the electronic structure [11–18,59–61]. The model parameters are provided by Ref. [19]. Surprisingly, the hole-doped phase diagram shows largely s-wave pairing as well as an AFM phase (see Fig. 10). Some d-wave pairing is also found; however, it requires strong screening strength $\alpha \approx 0.1$ to develop. AFM order is robust and remains stable even at $U_d = 4$ eV, highlighting the importance of rare-earth screening required for superconductivity in $LaNiO_2$. The smaller Γ pocket [19] implies pairing toward s-wave, but its robustness against U_d is not expected and this type of order is more subtle. Compared to $NdNiO_2$, the parameter range for d-wave pairing is strongly reduced in $LaNiO_2$, and s-wave pairing dominates the phase diagram. In addition to d- and s-wave SC phases, we observe nonvanishing of $(d + s)$-wave at the crossover between the two above symmetries. Although this exotic type of pairing is interesting, with the small cluster size used here we cannot argue that it is stable in the thermodynamic limit.

Figure 11 shows pairing overlaps and the spin-structure factor for electron-doped $LaNiO_2$. As for electron-doped $NdNiO_2$ (see Fig. 8), strong correlations enhance AFM order in the $x^2 - y^2$ orbital and allow coexisting s-wave pairing in the s-like band. At weak correlations, however, we now find d-wave superconductivity in the regime without AFM order, in contrast to electron-doped $NdNiO_2$. However, in stark contrast to the hole-doped scenarios, the d-wave pairs are composed almost exclusively of s electrons rather than $x^2 - y^2$. This result suggests that superconductivity in electron-doped $LaNiO_2$ would be possible.

V. SUMMARY AND CONCLUSIONS

We have used exact diagonalization to investigate an effective two-band model for infinite-layer nickelates, where the band with a strong Ni($d_{x^2-y^2}$) character can be expected to be more correlated than the one with a rather extended s-like wave function of mostly rare-earth character. We focus here on the interactions in both bands, especially their relative strength, which also tunes the highly relevant [19] interorbital interactions between the two orbitals. The latter give interband interactions and are responsible for the pairing.

On both ends, the very strongly correlated and the strongly screened regimes, the two-band model can be mapped onto a single Hubbard-like band. For (unrealistically) strong interactions, we find an AFM Mott insulator without tendencies to superconductivity. In the more realistic screened regime, the s-like band takes up some of the charge carriers, which can easily be accounted for effectively by adjusting the doping level of the correlated $x^2 - y^2$ band [26].

For intermediate screening, in contrast, the s-band hosts the doped holes forming s-wave pairs, so that it cannot be neglected. The situation broadly corresponds to a Kondo-lattice-like scenario, with the caveat that the "localized" $d_{x^2-y^2}$ spins can also move [4,25,32]. Hund's exchange coupling naturally yields ferromagnetic interaction between itinerant s carriers and $d_{x^2-y^2}$ spins, but it is interesting to note that s-wave pairing at stronger coupling was also obtained in a similar effective model with AFM spin-spin coupling [25].

The hopping parameters used were modeled on $NdNiO_2$, and we find that a self-doped $x^2 - y^2$ band can likely capture some regimes of a model for hole-doped $NdNiO_2$, while the s-like band would be expected to play a stronger role at electron doping. We also used a slight modification of the model in order to arrive at a model more appropriate to $LaNiO_2$ and

conclude that the *s*-like band can similarly be expected to play a stronger role. Electron doping enhances antiferromagnetism, and *s*-wave pairing due to the *s* orbital might then arise, while *d*-wave pairing is only found for $LaNiO_2$, but not for $NdNiO_2$. We find that the overall phase diagrams are similar for model parameters aiming at $NdNiO_2$ and $LaNiO_2$. However, a mapping onto a single Hubbard band is here applicable to a significantly reduced part of the parameter space in the case of $LaNiO_2$, with a much broader regime falling into the Kondo-lattice-like two-band regime. We thus conclude that many, but not necessarily all, aspects of Ni-based superconductors can be discussed in an effective one-band scenario, in agreement with Ref. [34].

Experimental evidence on pairing symmetry is at the moment not completely clear. Recent observation on both Nd- and La-based compounds suggests isotropic nodeless pairing in Nd nickelate while it is anisotropic nodeless or nodal + nodeless pairing in La nickelate [62]. Tunneling spectra in $Nd_{1-x}Sr_xNiO_2$ thin films have revealed *d*- as well as *s*-wave gaps [27]. Different surface termination has been conjectured to underlie this observation and our results might provide a rationalization: if termination reduces screening locally, it can push the system into the *s*-wave regime.

Note added. Recently we became aware of a two-band model study of nickelates by the Stanford group [63]. A common feature is the coexistence of a strongly correlated $x^2 - y^2$ orbital and a weakly correlated *s*-like orbital which supports the relevance of such a two-band model for the superconducting infinite-layer nickelates.

ACKNOWLEDGMENTS

We thank Wojtek Brzezicki, Andres Greco, and George A. Sawatzky for very insightful discussions. T.P. acknowledges Development and Promotion of Science and Technology Talents Project (DPST). A.M.O. acknowledges Narodowe Centrum Nauki (NCN, Poland) Project No. 2016/23/B/ST3/00839 and is grateful for support via the Alexander von Humboldt Foundation Fellowship (Humboldt-Forschungspreis).

[1] D. Li, K. Lee, B. Y. Wang, M. Osada, S. Crossley, H. R. Lee, Y. Cui, Y. Hikita, and H. Y. Hwang, Superconductivity in an infinite-layer nickelate, Nature (London) **572**, 624 (2019).

[2] M. Jiang, M. Berciu, and G. A. Sawatzky, Critical Nature of the Ni Spin State in Doped $NdNiO_2$, Phys. Rev. Lett. **124**, 207004 (2020).

[3] T. Plienbumrung, M. Daghofer, and A. M. Oleś, Interplay between Zhang-Rice singlets and high-spin states in a model for doped NiO_2 planes, Phys. Rev. B **103**, 104513 (2021).

[4] M. Hepting, D. Li, C. J. Jia, H. Lu, E. Paris, Y. Tseng, X. Feng, M. Osada, E. Been, Y. Hikita, Y.-D. Chuang, Z. Hussain, K. J. Zhou, A. Nag, M. Garcia-Fernandez, M. Rossi, H. Y. Huang, D. J. Huang, Z. X. Shen, T. Schmitt *et al.*, Electronic structure of the parent compound of superconducting infinite-layer nickelates, Nat. Mater. **19**, 381 (2020).

[5] H. Lu, M. Rossi, A. Nag, M. Osada, D. F. Li, K. Lee, B. Y. Wang, M. Garcia-Fernandez, S. Agrestini, Z. X. Shen, E. M. Been, B. Moritz, T. P. Devereaux, J. Zaanen, H. Y. Hwang, K.-J. Zhou, and W. S. Lee, Magnetic excitations in infinite-layer nickelates, Science **373**, 213 (2021).

[6] J. Q. Lin, P. Villar Arribi, G. Fabbris, A. S. Botana, D. Meyers, H. Miao, Y. Shen, D. G. Mazzone, J. Feng, S. G. Chiuzbăian, A. Nag, A. C. Walters, M. García-Fernández, K.-J. Zhou, J. Pelliciari, I. Jarrige, J. W. Freeland, J. Zhang, J. F. Mitchell, V. Bisogni *et al.*, Strong Superexchange in a $d^{9-\delta}$ Nickelate Revealed by Resonant Inelastic X-Ray Scattering, Phys. Rev. Lett. **126**, 087001 (2021).

[7] M. A. Hayward, M. A. Green, M. J. Rosseinsky, and J. Sloan, Sodium hydride as a powerful reducing agent for topotactic oxide deinteraction: Synthesis and characterization of the nickel (I) oxide $LaNiO_2$, J. Am. Chem. Soc. **121**, 8843 (1999).

[8] M. A. Hayward and M. J. Rosseinsky, Synthesis of the infinite layer Ni(I) phase $NdNiO_{2+x}$ by low temperature reduction of $NdNiO_3$ with sodium hydride, Solid State Sci. **5**, 839 (2003).

[9] L.-H. Hu and C. Wu, Two-band model for magnetism and superconductivity in nickelates, Phys. Rev. Res. **1**, 032046(R) (2019).

[10] Y.-H. Zhang and A. Vishwanath, Type-II *t*-*J* model in superconducting nickelate $Nd_{1-x}Sr_xNiO_2$, Phys. Rev. Res. **2**, 023112 (2020).

[11] P. Jiang, L. Si, Z. Liao, and Z. Zhong, Electronic structure of rare-earth infinite-layer $RNiO_2$ (R=La,Nd), Phys. Rev. B **100**, 201106(R) (2019).

[12] L. Si, W. Xiao, J. Kaufmann, J. M. Tomczak, Y. Lu, Z. Zhong, and K. Held, Topotactic Hydrogen in Nickelate Superconductors and Akin Infinite-Layer Oxides ABO_2, Phys. Rev. Lett. **124**, 166402 (2020).

[13] X. Wu, D. Di Sante, T. Schwemmer, W. Hanke, H. Y. Hwang, S. Raghu, and R. Thomale, Robust $d_{x^2-y^2}$-wave superconductivity of infinite-layer nickelates, Phys. Rev. B **101**, 060504(R) (2020).

[14] M. Klett, T. Schwemmer, S. Wolf, X. Wu, D. Riegler, A. Dittmaier, D. Di Sante, G. Li, W. Hanke, S. Rachel, and R. Thomale, From high T_c to low T_c: Multiorbital effects in transition metal oxides, Phys. Rev. B **104**, L100502 (2021).

[15] R. Zhang, C. Lane, B. Singh, J. Nokelainen, B. Barbiellini, R. S. Markiewicz, A. Bansil, and J. Sun, Magnetic and f-electron effects in $LaNiO_2$ and $NdNiO_2$ nickelates with cuprate-like $3d_{x^2-y^2}$ band, Commun. Phys. **4**, 118 (2021).

[16] E. Been, W.-S. Lee, H. Y. Hwang, Y. Cui, J. Zaanen, T. Devereaux, B. Moritz, and C. Jia, Electronic Structure Trends across the Rare-Earth Series in Superconducting Infinite-Layer Nickelates, Phys. Rev. X **11**, 011050 (2021).

[17] K. Higashi, M. Winder, J. Kuneš, and A. Hariki, Core-Level X-Ray Spectroscopy of Infinite-Layer Nickelate: LDA + DMFT Study, Phys. Rev. X **11**, 041009 (2021).

[18] A. S. Botana, K.-W. Lee, M. R. Norman, V. Pardo, and W. E. Pickett, Low valence nickelates: Launching the nickel age of superconductivity, Front. Phys. **9**, 813532 (2021).

[19] P. Adhikary, S. Bandyopadhyay, T. Das, I. Dasgupta, and T. Saha-Dasgupta, Orbital-selective superconductivity in a two-band model of infinite-layer nickelates, Phys. Rev. B **102**, 100501(R) (2020).

[20] Y. Nomura, M. Hirayama, T. Tadano, Y. Yoshimoto, K. Nakamura, and R. Arita, Formation of a two-dimensional single-component correlated electron system and band engineering in the nickelate superconductor $NdNiO_2$, Phys. Rev. B **100**, 205138 (2019).

[21] Y. Gu, S. Zhu, X. Wang, J. Hu, and H. Chen, A substantial hybridization between correlated Ni-d orbital and itinerant electrons in infinite-layer nickelates, Commun. Phys. **3**, 84 (2020).

[22] F. Lechermann, Multiorbital Processes Rule the $Nd_{1-x}Sr_xNiO_2$ Normal State, Phys. Rev. X **10**, 041002 (2020).

[23] T. Y. Xie, Z. Liu, C. Cao, Z. F. Wang, J. L. Yang, and W. Zhu, Microscopic theory of superconducting phase diagram in infinite-layer nickelates, Phys. Rev. B **106**, 035111 (2022).

[24] A. Kreisel, B. M. Andersen, A. T. Rømer, I. M. Eremin, and F. Lechermann, Superconducting Instabilities in Strongly Correlated Infinite-Layer Nickelates, Phys. Rev. Lett. **129**, 077002 (2022).

[25] Z. Wang, G.-M. Zhang, Y.-F. Yang, and F.-C. Zhang, Distinct pairing symmetries of superconductivity in infinite-layer nickelates, Phys. Rev. B **102**, 220501(R) (2020).

[26] M. Kitatani, L. Si, R. Arita, Z. Zhong, and K. Held, Nickelate superconductors—a renaissance of the one-band Hubbard model, npj Quantum Mater. **5**, 59 (2020).

[27] Q. Gu, Y. Li, S. Wan, H. Li, W. Guo, H. Yang, Q. Li, X. Zhu, X. Pan, Y. Nie, and H.-H. Wen, Single particle tunneling spectrum of superconducting $Nd_{1-x}Sr_xNiO_2$ thin films, Nat. Commun. **11**, 134502 (2020).

[28] Y. Nomura and R. Arita, Superconductivity in infinite-layer nickelates, Rep. Prog. Phys. **85**, 052501 (2022).

[29] A. S. Botana and M. R. Norman, Similarities and Differences between $LaNiO_2$ and $CaCuO_2$ and Implications for Superconductivity, Phys. Rev. X **10**, 011024 (2020).

[30] F. C. Zhang and T. M. Rice, Effective Hamiltonian for the superconducting Cu oxides, Phys. Rev. B **37**, 3759 (1988).

[31] H. Sakakibara, H. Usui, K. Suzuki, T. Kotani, H. Aoki, and K. Kuroki, Model Construction and a Possibility of Cupratelike Pairing in a New d^9 Nickelate Superconductor (Nd,Sr)NiO_2, Phys. Rev. Lett. **125**, 077003 (2020).

[32] G.-M. Zhang, Y.-f. Yang, and F.-C. Zhang, Self-doped Mott insulator for parent compounds of nickelate superconductors, Phys. Rev. B **101**, 020501(R) (2020).

[33] M. Rossi, H. Lu, A. Nag, D. Li, M. Osada, K. Lee, B. Y. Wang, S. Agrestini, M. Garcia-Fernandez, J. J. Kas, Y.-D. Chuang, Z. X. Shen, H. Y. Hwang, B. Moritz, K.-J. Zhou, T. P. Devereaux, and W. S. Lee, Orbital and spin character of doped carriers in infinite-layer nickelates, Phys. Rev. B **104**, L220505 (2021).

[34] F. Lechermann, Doping-dependent character and possible magnetic ordering of $NdNiO_2$, Phys. Rev. Mater. **5**, 044803 (2021).

[35] N. Marzari and D. Vanderbilt, Maximally localized generalized Wannier functions for composite energy bands, Phys. Rev. B **56**, 12847 (1997).

[36] I. Souza, N. Marzari, and D. Vanderbilt, Maximally localized Wannier functions for entangled energy bands, Phys. Rev. B **65**, 035109 (2001).

[37] P. Giannozzi, S. Baroni, N. Bonini, M. Calandra, R. Car, C. Cavazzoni, D. Ceresoli, G. L. Chiarotti, M. Cococcioni, I. Dabo, A. D. Corso, S. de Gironcoli, S. Fabris, G. Fratesi, R. Gebauer, U. Gerstmann, C. Gougoussis, A. Kokalj, M. Lazzeri, L. Martin-Samos *et al.*, QUANTUM ESPRESSO: A modular and open-source software project for quantum simulations of materials, J. Phys.: Condens. Matter **21**, 395502 (2009).

[38] P. Giannozzi, O. Andreussi, T. Brumme, O. Bunau, M. B. Nardelli, M. Calandra, R. Car, C. Cavazzoni, D. Ceresoli, M. Cococcioni, N. Colonna, I. Carnimeo, A. D. Corso, S. de Gironcoli, P. Delugas, R. A. DiStasio Jr., A. Ferretti, A. Floris, G. Fratesi, G. Fugallo *et al.*, Advanced capabilities for materials modelling with QUANTUM ESPRESSO, J. Phys.: Condens. Matter **29**, 465901 (2017).

[39] P. Giannozzi, O. Baseggio, P. Bonfà, D. Brunato, R. Car, I. Carnimeo, C. Cavazzoni, S. de Gironcoli, P. Delugas, F. Ferrari Ruffino, A. Ferretti, N. Marzari, I. Timrov, A. Urru, and S. Baroni, QUANTUM ESPRESSO toward the exascale, J. Chem. Phys. **152**, 154105 (2020).

[40] A. Dal Corso, Pseudopotentials periodic table: From H to Pu, Comput. Mater. Sci. **95**, 337 (2014).

[41] J. I. Budnick, B. Chamberland, D. P. Yang, C. Niedermayer, A. Golnik, E. Recknagel, M. Rossmanith, and A. Weidinger, Dependence of the Nèel-temperatures of La_2CuO_4 on Sr-doping studied by muon spin rotation, Europhys. Lett. **5**, 651 (1988).

[42] G. Pizzi, V. Vitale, R. Arita, S. Blügel, F. Freimuth, G. Géranton, M. Gibertini, D. Gresch, C. Johnson, T. Koretsune, J. Ibañez-Azpiroz, H. Lee, J.-M. Lihm, D. Marchand, A. Marrazzo, Y. Mokrousov, J. I. Mustafa, Y. Nohara, Y. Nomura, L. Paulatto *et al.*, Wannier90 as a community code: New features and applications, J. Phys.: Condens. Matter **32**, 165902 (2020).

[43] See Supplemental Material at http://link.aps.org/supplemental/10.1103/PhysRevB.106.134504 for the tight binding parameters of the models shown in Fig. 1, orbital electron densities, spin structure factor of the undoped system, and the ground state overlap as in Fig. 7.

[44] E. Koch, The Lanczos method, in *The LDA+DMFT Approach to Strongly Correlated Materials*, edited by E. Pavarini, E. Koch, D. Vollhardt, and A. Lichtenstein (Forschungszentrum Jülich, Jülich, 2011).

[45] T. Plienbumrung, M. Schmid, M. Daghofer, and A. M. Oleś, Character of doped holes in $Nd_{1-x}Sr_xNiO_2$, Condens. Matter **6**, 33 (2021).

[46] M. Shiroishi and M. Wadati, Integrable boundary conditions for the one-dimensional Hubbard model, J. Phys. Soc. Jpn. **66**, 2288 (1997).

[47] D. Poilblanc, Twisted boundary conditions in cluster calculations of the optical conductivity in two-dimensional lattice models, Phys. Rev. B **44**, 9562 (1991).

[48] W.-G. Yin and W. Ku, Flavor-twisted boundary condition for simulations of quantum many-body systems, Phys. Rev. B **80**, 180402(R) (2009).

[49] Y. Nomura, T. Nomoto, M. Hirayama, and R. Arita, Magnetic exchange coupling in cuprate-analog d^9 nickelates, Phys. Rev. Res. **2**, 043144 (2020).

[50] F. Lechermann, Late transition metal oxides with infinite-layer structure: Nickelates versus cuprates, Phys. Rev. B **101**, 081110(R) (2020).

[51] H. Eskes and A. M. Oleś, Two Hubbard Bands: Weight Transfer in Optical and One-Particle Spectra, Phys. Rev. Lett. **73**, 1279 (1994).

[52] H. Eskes, A. M. Oleś, M. B. J. Meinders, and W. Stephan, Spectral properties of the Hubbard bands, Phys. Rev. B **50**, 17980 (1994).

[53] A. Moreo, M. Daghofer, J. A. Riera, and E. Dagotto, Properties of a two-orbital model for oxypnictide superconductors: Magnetic order, B_{2g} spin-singlet pairing channel, and its nodal structure, Phys. Rev. B **79**, 134502 (2009).

[54] A. Nicholson, W. Ge, X. Zhang, J. Riera, M. Daghofer, A. M. Oleś, G. B. Martins, A. Moreo, and E. Dagotto, Competing Pairing Symmetries in a Generalized Two-Orbital Model for the Pnictide Superconductors, Phys. Rev. Lett. **106**, 217002 (2011).

[55] S. Ryee, H. Yoon, T. J. Kim, M. Y. Jeong, and M. J. Han, Induced magnetic two-dimensionality by hole doping in the superconducting infinite-layer nickelate Nd_{1-x} Sr_x NiO_2, Phys. Rev. B **101**, 064513 (2020).

[56] H.-S. Jin, W. E. Pickett, and K.-W. Lee, Proposed ordering of textured spin singlets in a bulk infinite-layer nickelate, Phys. Rev. Res. **2**, 033197 (2020).

[57] N. Kitamine, M. Ochi, and K. Kuroki, Designing nickelate superconductors with d^8 configuration exploiting mixed-anion strategy, Phys. Rev. Res. **2**, 042032(R) (2020).

[58] E. M. Nica, J. Krishna, R. Yu, Q. Si, A. S. Botana, and O. Erten, Theoretical investigation of superconductivity in trilayer square-planar nickelates, Phys. Rev. B **102**, 020504(R) (2020).

[59] D. Zhao, Y. B. Zhou, Y. Fu, L. Wang, X. F. Zhou, H. Cheng, J. Li, D. W. Song, S. J. Li, B. L. Kang, L. X. Zheng, L. P. Nie, Z. M. Wu, M. Shan, F. H. Yu, J. J. Ying, S. M. Wang, J. W. Mei, T. Wu, and X. H. Chen, Intrinsic Spin Susceptibility and Pseudogaplike Behavior in Infinite-Layer $LaNiO_2$, Phys. Rev. Lett. **126**, 197001 (2021).

[60] M. Islam, S. Koley, and S. Basu, Transport properties of the parent $LaNiO_2$, Eur. Phys. J. B **94**, 187 (2021).

[61] S. W. Zeng, C. J. Li, L. E. Chow, Y. Cao, Z. Zhang, C. S. Tang, X. Yin, Z. S. Lim, J. Hu, P. Yang, and A. Ariando, Superconductivity in infinite-layer lanthanide nickelates, Sci. Adv. **8**, eabl9927 (2022).

[62] L. E. Chow, S. K. Sudheesh, P. Nandi, S. W. Zeng, Z. T. Zhang, X. M. Du, Z. S. Lim, E. E. M. Chia, and A. Ariando, Pairing symmetry in infinite-layer nickelate superconductor, arXiv:2201.10038.

[63] C. Peng, H. C. Jiang, B. Moritz, T. P. Devereaux, and C. Jia, Superconductivity in a minimal two-band model for infinite-layer nickelates, arXiv:2110.07593.